This is a preprint, the final version is subject to change, of the American Mineralogist (MSA)
Cite as Authors (Year) Title. American Mineralogist, in press.
DOI: https://doi.org/10.2138/am-2019-6804

Revision 1

The oxidation state of sulfur in lunar apatite

Maryjo Brounce[1*], Jeremy Boyce[2], Francis M. McCubbin[2], Jennifer Humphreys[1], Justin Reppart[2], Edward Stolper[3], and John Eiler[3]

[1]Department of Earth Sciences, University of California Riverside, Riverside CA US 92521
[2]Astromaterials Research and Exploration Science Division, NASA Johnson Space Center, Houston, TX US
[3]Division of Geological and Planetary Sciences, California Institute of Technology, Pasadena CA
*corresponding author, email: mbrounce@ucr.edu

Abstract

Lunar apatites contain 100s-1000s ppm sulfur. This is puzzling because lunar basalts are thought to form in low oxygen fugacity (fO_2) conditions where sulfur can only exist in its reduced form (S^{2-}), a substitution not previously observed in natural apatite. We present measurements of the oxidation state of S in lunar apatites and associated mesostasis glass that show that lunar apatites and glass contain dominantly S^{2-}, whereas natural apatites from Earth are only known to contain S^{6+}. It is likely that many terrestrial and Martian igneous rocks contain apatites with mixed sulfur oxidation states. The S^{6+}/S^{2-} ratios of such apatites could be used to quantify the fO_2s at which they crystallized, given information on the portioning of S^{6+} and S^{2-} between apatite and melt and on the S^{6+}/S^{2-} ratios of melts as functions of fO_2 and melt composition. Such an well-oxybarometer based on this the oxidation state of S in apatite would have wide application.

Introduction

Lunar apatites, melt inclusions, and glass beads contain concentrations of H, C, S, and Cl that suggest that at least some portions of the lunar crust and/or mantle contain higher concentrations of these volatile elements than previously thought, and perhaps even in concentrations similar to those observed for Earth (Saal et al., 2008; Boyce et al. 2010; Greenwood et al. 2011; Hauri et al. 2011; Chen et al. 2015; McCubbin et al. 2015; Wetzel et al. 2015). This has led to significant recent interest in lunar volatiles and to efforts to explain these results in the context of models for the formation of the Moon. A puzzling aspect of the unexpectedly high volatile contents of lunar materials was the observation of 100s-1000s ppm S in apatite, similar to the levels observed in terrestrial igneous apatite (Boyce et al. 2010).

Terrestrial magmas typically formed at fO_2 levels 4-5 orders of magnitude higher than the iron-wüstite oxygen buffer (referred to as IW+4 to +5). At these fO_2s, sulfur dissolved in the silicate liquids from which terrestrial apatites crystallize is present as sulfate (i.e., SO_4^{2-}, or S^{6+})

and sulfide (i.e., S^{2-}), but it has been generally believed that the sulfur in terrestrial apatites is present entirely as sulfate (Fleet 2005), with the sulfate anion in the apatite substituting for the phosphate anionic group, coupled with SiO_4^{4-} or Na^+ to maintain charge balance (Pan and Fleet 2002). However, lunar rocks reflect much lower fO_2 conditions, including at the point of apatite saturation and crystallization. Lunar apatites crystallize in the interstices of lunar basalts from late-stage, highly differentiated liquids, since only in such liquids does phosphorus reach sufficient concentrations for the liquids to become saturated with respect to apatite. The fO_2 of these late-stage liquids in lunar basalts are constrained from petrographic descriptions of the phases present in the interstices (e.g., coexistence of Fe-metal, ulvospinel, ilmenite, and sometimes fayalite and/or silica) and are as low as IW-1 (e.g., El Goresy 1976). This is more than 4 orders of magnitude lower than the fO_2s required to begin to stabilize sulfate in basaltic and andesitic liquids (~IW+3.5; Botcharnikov et al. 2010; Jugo et al. 2010), and more than 3 orders of magnitude lower than needed in Fe-free or Fe-poor soda-lime, $K_2Si_4O_9$, albite, and haplo-trondhjemite liquids (~IW+2.5; Klimm et al. 2012). Thus, under the reducing conditions of lunar petrogenesis, it is anticipated that nearly all S dissolved in the interstitial silicate melts in these lunar magmas will be dissolved as sulfide (S^{2-}), and that crystalline phases in equilibrium with the interstitial silicate melts likely contain nearly entirely sulfide. Since at the time of the discovery of 100s-1000s ppm S in lunar apatites sulfur was only known to be present in naturally occurring apatite as sulfate groups, it was not clear how to explain the incorporation of sulfur in lunar apatites (Boyce et al. 2010).

Boyce et al. (2010) speculated that the elevated S abundances of lunar apatites under conditions that are so reducing as to be highly unfavorable to stabilization of significant sulfate in the liquids with which the apatites coexisted was due to sulfide substitution into the column anion site in apatite where F^-, OH^-, and Cl^- anions normally sit. Although this hypothesized substitution has until now not been observed in natural apatites, in support of their speculation, Boyce et al. (2010) pointed out that fully S^{2-}-substituted apatites had been synthesized experimentally (Suitch et al. 1986; Taitai and Lacout 1989; Henning et al. 2000), and since then, apatites that exhibit S-XANES spectral evidence for both sulfide and sulfate (Konecke et al. 2017a) have been synthesized. The speculation that this occurs at the column anion site also is supported by *ab initio* calculations, which show that this substitution of S^{2-} is most energetically favorable in chloride-bearing apatites (Kim et al. 2017). If natural apatite can simultaneously incorporate both oxidized and reduced sulfur (S^{6+} and S^{2-}), it is possible that their proportions could be sensitive to the S^{6+}/S^{2-} ratio of the apatite growth environment, and therefore could provide a proxy for the fO_2 at which the apatites formed. This possibility is of interest because apatites are a common

igneous phase in a variety of rocks from Earth, Moon, and other planets and the determination of fO_2 is a topic of considerable interest and importance (e.g., Haggerty and Meyer 1970; Taylor et al. 1972, 2004; Sato et al. 1973; Sato 1979; Carmichael, 1991; Steele et al. 1992; Herd et al. 2002; Karner et al. 2006; Wadhwa et al. 2008; Kelley and Cottrell, 2009; Jugo et al. 2010; Wetzel et al. 2013; Brounce et al. 2017; Konecke et al. 2017a). In this paper, we report the results of x-ray absorption near edge structure spectroscopy (S-XANES, see SI Appendix) on S-bearing lunar apatite (from basalt samples 10044 and 12039) and terrestrial igneous apatite (from Durango) and demonstrate that S^{2-} dominates in the lunar apatites but is undetectable in the terrestrial apatite.

Sample Description

Sample 12039 is a 3.2 ± 0.05 billion year old, low-TiO_2 basalt (Nyquist et al. 1979). Sample 10044 is a ~3.71-3.73 billion year old, high-TiO_2 basalt (Turner 1970; Guggisberg et al. 1979). Both rocks are inferred to have been derived from lava flows (Klein 1972). They are slightly vesiculated (< 1%) and dominated by compositionally zoned and skeletal pyroxene, plagioclase, and ilmenite (Klein 1972). For both samples, fractionation of the basaltic magma due to crystallization at low fO_2 produced Fe-rich late-stage liquids, which then separated into two immiscible liquids upon further crystallization – one very Si-rich, Fe-poor melt that occurs as quenched glass containing 78 wt% SiO_2, 0.5 wt% FeO*, 3.2 wt% K_2O, 4.48 wt% CaO, and <0.03 wt% MgO (versus the bulk lava with ~47 wt% SiO_2, 20.39 wt% FeO*, 0.11 wt% K_2O, 11.6 wt% CaO, and ~8.6 wt% MgO; Boyce et al. 2014), and another lower silica, Fe-rich melt (SiO_2 ~47.8 wt%, FeO* ~ 20 wt%, K_2O ~0.3 wt%, CaO ~11.2 wt%, MgO ~ 2.3 wt%; Roedder and Weiblen 1970; Pernet-Fisher et al. 2014). Apatite can be in contact with either glass in both samples (Pernet-Fisher et al. 2014), and recent experimental data indicate that the composition of apatites among conjugate liquids are indistinguishable with respect to major and minor elements in systems that undergo silicate-liquid immiscibility (McCubbin and Ustunisik 2018). Sulfide blebs are also associated with silicate glass in the mesostasis in both samples, suggesting that apatites analyzed in this study crystallized from and equilibrated with a sulfide-saturated silicate melt (Fig 1-3). Features such as rounded silicate glass-sulfide contacts (e.g., rounded sulfide/K-glass contact in upper right region of Fig 1a, b) indicate that the sulfide was molten. The mesostasis in the thin section of sample 12039 studied here (thin section 4) also contains K,Si-rich glass, K,Ba-feldspar, troilite (distinguished from sulfide on the basis of the shape of their XANES spectra, SFig 1), plagioclase, and pyroxenes (e.g., Fig 1). Other studies of sample 12039 also report tranquillityite, native iron, cristobalite, and tridymite in the mesostasis (Bunch et al. 1972). The mesostasis in sample 10044 studied here (thin section 33) contains crystallized troilite,

plagioclase, fayalite, SiO_2, and pyroxene (e.g., Fig 3). Other studies of sample 10044 also report baddeleyite, ulvöspinel, tranquillityite, K,Ba-feldspar in hand sample, as well as K,Si-rich glass and devitrified high-Fe glass, the last two of which are interpreted as being immiscible liquids (Beaty and Albee 1978). Apatites in thin sections of both rocks have igneous textures as indicated by equant and skeletal grains with central cavities filled with glass, as well as compositionally zoned crystals (see Figs 1 and 3; Piccoli and Candela 2002). These apatites contain 100s-1000s ppm S (determined via electron probe; Greenwood et al. 2011). Apatite grains in sample 12039 have been shown to be zoned with respect to F, Cl, SiO_2, and S, which was hypothesized to reflect variations in the composition of a residual melt during apatite crystallization (Greenwood et al. 2011).

Durango apatite is from volcanogenic deposits near Durango, Mexico and ins associated with magnetite in gas cavities and open breccias in sheeted flows and flow breccias from Cerro de Mercado. Halogen-rich gases are thought to have streamed through and further oxidized magnetite to hematite, setting the fO_2 conditions under which Durango apatite formed at >IW+6 (Lyons 1988). At these fO_2s, sulfur is expected in solution as S^{6+} (Botcharnikov et al. 2010; Jugo et al. 2010; Klimm et al. 2012).

Results

The measured $S^{6+}/\Sigma S$ ratios vary between 0 and 45% in six lunar apatite grains in thin section 12039,4 vary between 0 and 45% (Fig 1, 2, SFig 2, 3; Supplementary Table 1) and between 0 and 32% in two apatite grains in thin section 10044,33 (Fig 3, SFig4; Supplementary Table 1). The sulfur concentrations of the K,Si-rich mesostasis glass touching measured apatites in sample 12039 contain 69-107 ppm S, and two S-XANES analyses of the mesostasis glass demonstrate that sulfur is present in the mesostasis have the characteristic spectral features of dissolved S^{2-} in terrestrial basaltic liquids (e.g., Jugo et al. 2010; Brounce et al. 2017) but no spectral evidence for the presence of S^{6+} dissolved in the glass, resulting in a $S^{6+}/\Sigma S = 0\%$ (Fig 2). More than half of all measurements on apatite (28 analyses out of 48 total analyses) have $S^{6+}/\Sigma S < 3\%$, which we consider to be indistinguishable from 0% (see SI Appendix). This is in contrast with our analyses of Durango apatite (the representative of terrestrial apatite considered in this study), which shows the characteristic spectral features of S^{6+}, but no spectral evidence for the presence of S^{2-}, resulting in a $S^{6+}/\Sigma S = 100\%$ (SFig 1).

Sulfur abundances of the same apatites and glasses were measured via electron microprobe (see SI Appendix) and vary from below the detection limit (~20 ppm based on

measurements of nearby silicate minerals that are nominally free of sulfur) up to 500 ppm in thin section 12039,4 (SFig 2, 3, 5; Supplementary Table 1) and up to ~350 ppm in thin section 10044,33 (SFig 4, 6; Supplementary Table 1). Individual apatite grains are heterogeneous with respect to sulfur. Where analyzed, the sulfur abundances of the mesostasis glass in 12039,4 range from below the detection limit to ~100 ppm S (SFig 5; Supplementary Table 1).

Discussion

In apatites from both 12039 and 10044, the locations of analyses that yield $S^{6+}/\Sigma S > 3\%$ correspond with the presence of fractures and/or pits (Fig 1-3; SFig 2-4). This suggests that the S^{6+} observed in these S-XANES spectra may not reflect primary sulfur incorporated into the apatite when it crystallized, but rather is either primary sulfide altered to sulfate or sulfur of secondary origin. Although it is possible that some portion of the S^{6+} signal is derived from the epoxies used in making the thin sections, the sharp absorption feature that appears at ~2474 eV in the epoxies, which does not appear in the mineral standards or in apatite measurements, and the low intensity of the S^{6+} peak in the epoxy (~2482 eV; SFig 1) in each thin section limits the proportion that epoxy can contribute to the measured absorption spectra in apatite to < 1% (SFig 1). There also could be secondary sulfate-bearing materials precipitated in the fractures and pits of the thin sections of these rocks, but, if so, we have no basis for evaluating whether these could be of terrestrial or lunar origin. Chlorine isotope measurements of the so called "rusty" rock (Apollo sample 66095) suggest a lunar origin for oxidation and hydration induced, Cl-bearing minerals observed in Apollo 16 samples (Shearer et al. 2014), and it is thus possible that apatites in Apollo 11 and 12 samples studied here are susceptible to similar fumerolic alteration (e.g., Konecke et al. 2017b). On the other hand, measurements of the hydrogen isotope contents of lunar apatites near fractures reveal distinctly terrestrial surface water signatures (Greenwood et al. 2011), and this terrestrial water contamination may have been associated with deposition of micro-to-nano-scale S^{6+}-bearing phases. Finally, while all spectra that indicate $S^{6+}/\Sigma S > 3\%$ are near fractures and pits in the thin section, there are some spectra that are near fractures or pits and do not have significantly elevated $S^{6+}/\Sigma S$ ratios (Fig 1-3; SFig 2-4), suggesting that if the oxidized sulfur we have detected is from secondary sulfate-bearing materials in the fractures and pits of these thin sections, these sulfates are heterogeneously distributed. The key point is that analyses taken far from fractures and pits are uniformly lacking in S^{6+} absorption features (i.e., $S^{6+}/\Sigma S < 3\%$; e.g., Fig 3).

Lunar basalts are also variably affected by subsolidus reactions, for instance, as the result of interaction between their primary mineral assemblages and implanted solar wind hydrogen (e.g., sample 14053; Taylor et al. 2004). It is possible that some or all of the S^{2-} found in lunar apatites measured in this study was formed as the result of interaction between solar wind hydrogen and sulfur-bearing phases such as troilite (i.e., reducing Fe^{2+} to Fe^0 and making S^{2-} available to diffuse into pre-existing, sulfide-poor or -free apatite), and thus do not record the fO_2 of the igneous system described by the bulk rock. However, unlike apatite grains in sample 14053, where solar wind implantation may have lowered the hydrogen isotopic compositions of apatite grains in thin section from their primary values, the hydrogen isotopic compositions of apatite grains in samples 12039 and 10044 are higher (δD in apatites from 14053 vary from -100 to -200‰, from 12039 vary from +400 to +1000‰, from 10044 vary from +550 to +750‰; (Greenwood et al. 2011). Solar wind has low D/H ratios, so the D-enrichment of apatite in the rocks studied here limits the extent to which solar wind implantation influenced incorporation of S^{2-} into apatite. Apollo rocks are also variably influenced by impact-related metamorphism and metasomatism. For example, abundant apatite found in granulite 79215 were hypothesized to be condensed from a halogen-rich vapor (Treiman et al. 2014). However, apatite grains in the mare basalts studied here have distinctly igneous textures, including being embayed by and displaying resorption textures with the mesostasis melt (e.g., Fig 1, 3, SFig 2-4), indicating that apatite was present in the rock at the time the mesostasis was liquid. Our preferred interpretation of S^{2-} -only lunar apatites in this study is that this reflects the low fO_2 conditions of the magma at the time of apatite crystallization.

The mesostasis glass in sample 12039 contains 70-110 ppm sulfur and that sulfur is entirely present as S^{2-} (Supplementary Table 1, SFig 5). For Apollo 12 basalts, experiments and petrographic observations suggest that olivine and pigeonite are the liquidus phases at an $fO_2 \sim$ IW (Green et al. 1971; Rhodes et al. 1977). The presence of Fe-metal and troilite, and in some cases fayalite, Fe-metal, and silica, or of ulvöspinel, Fe-metal, and ilmenite in the mesostasis reflects $fO_2 \leq$ IW-1, consistent with differentiation (i.e., low-pressure crystallization and degassing) having led to a decrease of at least an order of magnitude in fO_2. This could be driven by degassing of a C-H-O-S vapor, which has been shown to be an effective means of reducing the fO_2 of Hawaiian magmas by ~1 order of magnitude (Moussallam et al. 2016; Helz et al. 2017; Brounce et al. 2017), and has been suggested for lunar basalts previously (Brett 1976). Based on these previous results, the liquids from which lunar apatites in basalts crystallized clearly experienced fO_2s at which sulfur is expected in solution as S^{2-}, as confirmed by our S-XANES analyses of the mesostasis glass from sample 12039 and consistent with our S-XANES

measurements on apatite far from cracks and pits from both 12039 and 10044 (Fig 1-4). These latter results contrast with our S-XANES results on the Durango apatite, which has $S^{6+}/\Sigma S$ = 100% (SFig 1).

Paired glass-apatite measurements in sample 12039 enable an estimate of the partition coefficient of sulfide for apatite coexisting with K-Si-rich mesostasis melt. Taking the average sulfide concentration of the mesostasis glass in sample 12039 (88 ppm; Supplementary Table 1) and of the apatite measurements in the same thin section (176 ppm, assuming that $S^{6+}/\Sigma S$ of lunar apatite at the time of apatite crystallization is zero), then for conditions appropriate for apatite crystallization in the mesostasis of sample 12039, $D_{S2-}^{ap/liq} \sim 2 \pm 1$. Importantly, however, apatite-melt coefficients may vary as a function of temperature, pressure, melt composition, apatite composition, and/or oxygen fugacity, so the combined effects of these parameters must be investigated further before being applied broadly to determine sulfur abundaces of coexisting melt from apatite S^{2-} abundances.

Implications

We have documented the occurrence of S^{2-} -only apatite in nature (Fig 1, 3 SFig 3, SFig 4). Although not unexpected from the experimental synthesis of sulfoapatites, *ab initio* calculations, and recent synthesis of mixed S^{6+}/S^{2-} apatites, this is the first documentation of its natural occurrence. This observation confirms speculation of Boyce et al. (2010) that the elevated S contents of lunar apatites crystallized from melts that record fO_2s at which silicate melts are expected to have only S^{2-} are due to the ability of S^{2-} to partition into the apatite mineral structure. Finally, this study, in combination with the recent experimental work of Konecke et al. (2017a, b), suggest that a S-in-apatite oxybarometer could be developed and applied to igneous rocks from a variety of planetary bodies in our solar system.

The $S^{6+}/\Sigma S$ of an individual silicate melt transitions from 0% to 100% over ~two orders of magnitude in fO_2. The range over which this transition occurs for an individual melt depends on its major element composition, i.e., the midpoint of this transition for the melts for which this transition has been measured varies from QFM-0.5 (IW+3) to QFM+1 (IW+4.5) (Botcharnikov et al. 2010; Jugo et al. 2010; Klimm et al. 2012). Apatites coexisting with a given melt over the fO_2 range of this transition are anticipated to contain both S^{6+} and S^{2-} and thus could be used to quantify the fO_2 of the system at the time of apatite crystallization. In detail the fO_2 dependence of the transition in $S^{6+}/\Sigma S$ for apatites coexisting with melt undergoing the same transition will depend on the individual partition coefficients of S^{2-} and S^{6+} between apatite and melt and the

major element composition of the melt (including the oxidation states of other heterovalent elements). Thus, development of an oxybarometer based on the $S^{6+}/\Sigma S$ of apatite would require experimental work to determine the individual partition coefficients of S^{2-} and S^{6+} between apatite and melt, and a quantification of the extent to which those partition coefficients vary as a function of pressure, temperature, oxygen fugacity, melt composition, and apatite composition. Although such experiments and measurements will probably not be simple, given the widespread occurrence of apatite in igneous rocks from Earth and other planets, and the interest in the fO_2s at which they formed (and their variations), such an oxybarometer would likely be useful. In particular, given the fO_2 range over which this transition is expected to occur for terrestrial magmas based on their major element compositions (Botcharnikov et al. 2010; Jugo et al. 2010), the fO_2 ranges of terrestrial magmas (Carmichael 1991), and the capacity of XANES for measurements of sulfide/sulfate ratios in experimental and natural glasses (Brounce et al. 2017), S-XANES measurements can be expected to readily detect sulfide-dominated apatites, mixed sulfide-sulfate apatites, and sulfate-dominated apatites (as in the case for the Durango apatite we studied) in terrestrial igneous rocks and that these results can, with appropriate experimental calibration, be used quantitatively as an apatite oxybarometer for igneous rocks ranging in composition from basalt to rhyolite. In addition to Earth and the Moon, apatites are found in lavas from planetary bodies distributed throughout the solar system (McCubbin and Jones 2015) and an apatite-based oxybarometer could be useful in constraining the fO_2 of lavas from Mars and the howardite-eucrite-diogenite parent body (e.g., Herd et al. 2002; Shearer et al. 2006; Wadhwa 2008).

Finally, we note that S^{2-} likely partitions into the column anion site in apatite as a substitution for two F^-, Cl^-, and/or OH^- anions. Thus, the abundance of S^{2-} in apatites may be useful in studies seeking to constrain the abundance of F, Cl, and H_2O in magmas based on their concentrations in apatite.

Acknowledgments

We thank A. Lanzirotti and M. Newville for assistance in beamline operations at the Advanced Photon Source, Argonne National Laboratory (APS ANL). This research was performed at GeoSoilEnviroCARS (The University of Chicago, Sector 13), APS ANL. GeoSoilEnviroCARS is supported by the National Science Foundation – Earth Sciences (EAR-1634415) and Department of Energy – GeoSciences (DE-FG02-94ER14466). This research used resources of APS, a US Department of Energy (DOE) Office of Science user facility operated for the DOE Office of

Science by ANL under Contract No. DE-AC02-06CH11357. Support for this research was provided by NASA's Planetary Science Research Program. We also thank the curatorial staff at NASA Johnson Space Center for allocations of Apollo samples for this study.

References cited

Albarède F., Albalat E., and Lee C.T.A. (2014) An intrinsic volatility scale relevant to the Earth and Moon and the status of water in the Moon. Meteoritics & Planetary Science, 50, 568–577.

Beaty, D.W., and Albee, A.L. (1978) Comparative petrology and possible genetic relations among the Apollo 11 basalts. Proceedings of the Ninth Planetary Science Conference, 1, 359–463.

Botcharnikov, R.E., Linnen, R.L., Wilke, M., Holtz, F., Jugo, P.J., and Berndt, J. (2010) High gold concentrations in sulphide-bearing magma under oxidizing conditions. Nature Geoscience, 4, 112.

Boyce, J.W., Liu, Y., Rossman, G.R., Guan, Y., Eiler, J.M., Stolper, E.M., and Taylor, L.A. (2010) Lunar apatite with terrestrial volatile abundances. Nature, 466, 466.

Boyce, J.W., Tomlinson, S.M., McCubbin, F.M., Greenwood, J.P., and Treiman, A.H. (2014) The Lunar Apatite Paradox. Science, 344, 400.

Brett, R. (1976) Reduction of mare basalts by sulfur loss. Geochimica et Cosmochimica Acta, 40, 997–1004.

Brounce, M., Stolper, E., and Eiler, J. (2017) Redox variations in Mauna Kea lavas, the oxygen fugacity of the Hawaiian plume, and the role of volcanic gases in Earth's oxygenation. Proceedings of the National Academy of Sciences.

Bunch T. E., Keils Klaus, and Prinz Martin (1972) MINERALOGY, PETROLOGY AND CHEMISTRY OF LUNAR ROCK 12039. Meteoritics, 7, 245–255.

Carmichael, I.S.E. (1991) The redox states of basic and silicic magmas: a reflection of their source regions? Contributions to Mineralogy and Petrology, 106, 129–141.

Chen, Y., Zhang, Y., Liu, Y., Guan, Y., Eiler, J., and Stolper, E.M. (2015) Water, fluorine, and sulfur concentrations in the lunar mantle. Earth and Planetary Science Letters, 427, 37–46.

Cottrell, E., Lanzirotti, A., Mysen, B., Birner, S., Kelley, K.A., Botcharnikov, R., Davis, F.A., and Newville, M. (2018) A Mossbauer-based XANES calibration for hydrous basalt glasses reveals radiation-induced oxidation of Fe. American Mineralogist, 103, 489–501.

El Goresy, A. (1976) Oxide minerals in lunar rocks. Reviews in Mineralogy and Geochemistry, 3, 47–72.

Fleet, M.E. (2005) Xanes spectroscopy of sulfur in Earth materials. The Canadian Mineralogist, 43, 1811–1838.

Green, D.H., Ringwood, A.E., Ware, N.G., Hibberson, W.O., Major, A., and Kiss, E. (1971) Experimental petrology and petrogenesis of Apollo 12 basalts. Proceedings of the Second Planetary Science Conference, 1, 601–615.

Greenwood, J.P., Itoh, S., Sakamoto, N., Warren, P., Taylor, L., and Yurimoto, H. (2011) Hydrogen isotope ratios in lunar rocks indicate delivery of cometary water to the Moon. Nature Geoscience, 4, 79.

Guggisberg, S., Eberhardt, P., Geiss, J., Grogler, N., and Stettler, A. (1979) Classification of the Apollo-11 mare basalts according to Ar^{39}-Ar^{40} ages and petrological properties. Proceedings of the Tenth Planetary Science Conference, 1–39.

315 Haggerty, S.E., and Meyer, H.O.A. (1970) Apollo 12: Opaque oxides. Earth and Planetary Science Letters, 9, 379–
316 387.

317 Hauri, E.H., Weinreich, T., Saal, A.E., Rutherford, M.C., and Van Orman, J.A. (2011) High Pre-Eruptive Water
318 Contents Preserved in Lunar Melt Inclusions. Science, 333, 213.

319 Helz, R.T., Cottrell, E., Brounce, M.N., and Kelley, K.A. (2017) Olivine-melt relationships and syneruptive redox
320 variations in the 1959 eruption of Kilauea volcano as revealed by XANES. Journal of Volcanology and
321 Geothermal Research, 333-1-14.
322
323 Henning, P.A., Adolfsson, E., and Grins, J. (2000) The chalcogenide phosphate apatites $Ca_{10}(PO_4)_6S$, $Sr_{10}(PO_4)_6S$,
324 $Ba_{10}(PO_4)_6S$ and $Ca_{10}(PO_4)_6Se$. Zeitschrift fur Kristallographie - Crystalline Materials, 215, 226–230.

325 Herd, C.D.., Borg, L.E., Jones, J.H., and Papike, J.J. (2002) Oxygen fugacity and geochemical variations in the
326 martian basalts: implications for martian basalt petrogenesis and the oxidation state of the upper mantle of
327 Mars. Geochimica et Cosmochimica Acta, 66, 2025–2036.

328 Jugo, P.J., Wilke, M., and Botcharnikov, R.E. (2010) Sulfur K-edge XANES analysis of natural and synthetic basaltic
329 glasses: Implications for S speciation and S content as function of oxygen fugacity. Geochimica et
330 Cosmochimica Acta, 74, 5926–5938.

331 Karner, J.M., Sutton, S.R., Papike, J.J., Shearer, C.K., Jones, J.H., and Newville, M. (2006) Application of a new
332 vanadium valence oxybarometer to basaltic glasses from the Earth, Moon, and Mars. American
333 Mineralogist, 91, 270–277.

334 Kelley, K.A. and Cottrell, E. (2009) Water and the oxidation state of subduction zone magmas. Science, 325, 605-
335 607.
336
337 Kim, Y., Konecke, B., Fiege, A., Simon, A., and Becker, U. (2017) An ab-initio study of the energetics and geometry
338 of sulfide, sulfite, and sulfate incorporation into apatite: The thermodynamic basis for using this system as
339 an oxybarometer. American Mineralogist, 102, 1646–1656.

340 Klein, C. (1972) Lunar materials: Their mineralogy, petrology and chemistry. Earth-Science Reviews, 8, 169–204.

341 Klimm, K., Kohn, S.C., and Botcharnikov, R.E. (2012) The dissolution mechanism of sulphur in hydrous silicate
342 melts. II: Solubility and speciation of sulphur in hydrous silicate melts as a function of fO2. Chemical
343 Geology, 322–323, 250–267.

344 Konecke, B.A., Fiege, A., Simon, A.C., Parat, F., and Stechern, A. (2017a) Co-variability of S^{6+}, S^{4+}, and S^{2-} in
345 apatite as a function of oxidation state: Implications for a new oxybarometer. American Mineralogist, 102,
346 548–557.

347 Konecke, B.A., Fiege, A., Simon, A.C., and Holtz, F. (2017b) Cryptic metasomatism during late-stage lunar
348 magmatism implicated by sulfur in apatite. Geology, 45, 739–742.

349 Lyons, J.I. (1988) Volcanogenic iron oxide deposits, Cerro de Mercado and vicinity, Durango. Economic Geology,
350 83, 1886–1906.

351 McCubbin F. M., Jolliff B. L., Nekvasil H., Carpenter P. K., Zeigler R. A., Steele A., Elardo S. M., and Lindsley D.
352 H. (2011) Fluorine and chlorine abundances in lunar apatite: Implications for heterogeneous distributions of
353 magmatic volatiles in the lunar interior. Geochimica Et Cosmochimica Acta 75, 5073-5093.
354
355 McCubbin, F.M., and Jones, R.H. (2015) Extraterrestrial Apatite: Planetary Geochemistry to Astrobiology. Elements,
356 11, 183-188.
357
358 McCubbin, F.M., Steele, A., Nekvasil, H., Schnieders, A., Rose, T., Fries, M., Carpenter, P.K. and Jolliff, B.L.
359 (2010) Detection of structurally bound hydroxyl in fluorapatite from Apollo mare basalt 15058,128 using
360 TOF-SIMS. American Mineralogist 95, 1141-1150.

361

McCubbin, F.M., Vander Kaaden, K.E., Tartèse, R., Klima, R.L., Liu, Y., Mortimer, J., Barnes, J.J., Shearer, C.K., Treiman, A.H., Lawrence, D.J., and others (2015) Magmatic volatiles (H, C, N, F, S, Cl) in the lunar mantle, crust, and regolith: Abundances, distributions, processes, and reservoirs†. American Mineralogist, 100, 1668–1707.

McCubbin, F.M. and Ustunisik, G. (2018) Experimental investigation of F and Cl partitioning between apatite and Fe-rich basaltic melt at 0 GPa and 950-1050°C: Evidence for steric controls on apatite-melt exchange equilibria in OH-poor apatite. American Mineralogist, 103, in press.

Moussallam, Y., Edmonds, M., Scaillet, B., Peters, N., Gennaro, E., Sides, I., and Oppenheimer, C. (2016) The impact of degassing on the oxidation state of basaltic magmas: A case study of Kīlauea volcano. Earth and Planetary Science Letters, 450, 317–325.

Nyquist, L.E., Shih, C.-Y., Wooden, J.L., Bansal, B.M., and Wiesmann, H. (1979) The Sr and Nd isotopic record of Apollo 12 basalts: Implications for lunar geochemical evolution. Proceedings of the Tenth Planetary Science Conference, 77–114.

Pan, Y., and Fleet, M.E. (2002) Compositions of the apatite-group minerals: substitution mechanisms and controlling factors. Reviews in Mineralogy and Geochemistry, 48, 13–49.

Pernet-Fisher, J.F., Howarth, G.H., Liu, Y., Chen, Y., and Taylor, L.A. (2014) Estimating the lunar mantle water budget from phosphates: Complications associated with silicate-liquid-immiscibility. Geochimica et Cosmochimica Acta, 144, 326–341.

Piccoli, P., and Candela, P.A. (2002) Apatite in igneous systems. Reviews in Mineralogy and Geochemistry, 48, 255–292.

Rhodes, J.M., Blanchard, D.P., Dungan, M.A., Brannon, J.C., and Rodgers, K.V. (1977) Chemistry of Apollo 12 Mare basalts: Magma types and fractionation processes. Proceedings of the Eighth Planetary Science Conference, 1, 1305–1338.

Roedder, E., and Weiblen, P.W. (1970) Silicate Liquid Immiscibility in Lunar Magmas, Evidenced by Melt Inclusions in Lunar Rocks. Science, 167, 641.

Saal, A.E., Hauri, E.H., Cascio, M.L., Van Orman, J.A., Rutherford, M.C., and Cooper, R.F. (2008) Volatile content of lunar volcanic glasses and the presence of water in the Moon's interior. Nature, 454, 192-195.

Sato, M. (1979) The driving mechanism of lunar pyroclastic eruptions inferred from the oxygen fugacity behavior of Apollo 17 orange glass. Proceedings of the Tenth Planetary Science Conference, 311–325.

Sato, M., Hickling, N.L., and McLane, J., E. (1973) Oxygen fugacity values of Apollo 12, 14, and 15 lunar samples and reduced state of lunar magmas. Proceedings of the Fourth Lunar Science Conference, 1, 1061–1079.

Shearer, C.K., McKay, G., Papike, J.J., and Karner, J.M. (2006) Valence state partitioning of vanadium between olivine-liquid: Estimates of the oxygen fugacity of Y980459 and application to other olivine-phyric martian basalts. American Mineralogist, 91, 1657–1663.

Shearer, C.K., Sharp, Z.D., Burger, P.V., McCubbin, F.M., Provencio, P.P., Brearley, A.J., and Steele, A. (2014) Chlorine distribution and its isotopic composition in "rusty rock" 66095. Implications for volatile element enrichments of "rusty rock" and lunar soils, origin of "rusty" alteration, and volatile element behavior on the Moon. Geochimica et Cosmochimica Acta, 139, 411–433.

Steele, A.M., Colson, R.O., Korotev, R.L., and Haskin, L.A. (1992) Apollo 15 green glass: Compositional distribution and petrogenesis. Geochimica et Cosmochimica Acta, 56, 4075–4090.

Suitch, P.R., Taitai, A., Lacout, J.L., and Young, R.A. (1986) Structural consequences of the coupled substitution of Eu,S in calcium sulfoapatite. Journal of Solid State Chemistry, 63, 267–277.

Taitai, A., and Lacout, J.L. (1989) On the coupled introduction of Eu^{3+} and S^{2-} ions into strontium apatites. Journal of Physics and Chemistry of Solids, 50, 851–855.

Taylor, L.A., Williams, R.J., and McCallister, R.H. (1972) Stability relations of ilmenite and ulvöspinel in the Fe-Ti-O system and application of these data to lunar mineral assemblages. Earth and Planetary Science Letters, 16, 282–288.

Taylor, L.A., Patchen, A., Mayne, R.G., and Taylor, D.-H. (2004) The most reduced rock from the moon, Apollo 14 basalt 14053: Its unique features and their origin. American Mineralogist, 89, 1617–1624.

Treiman, A.., Boyce, J.W., Gross, J., Gao, Y., Eiler, J.M., and Stolper, E.M. (2014) Phosphate-halogen metasomatism of lunar granulite 79215: Impact-induced fractionation of volatiles and incompatible elements. American Mineralogist, 99, 1860–1870.

Turner, G. (1970) Argon-40/ Argon-39 Dating of Lunar Rock Samples. Science, 167, 466.

Wadhwa, M. (2008) Redox conditions on small bodies, the Moon and Mars. Reviews in Mineralogy and Geochemistry, 68, 493–510.

Wetzel, D.T., Rutherford, M.J., Jacobsen, S.D., Hauri, E.H., and Saal, A.E. (2013) Degassing of reduced carbon from planetary basalts. Proceedings of the National Academy of Sciences, 110, 8010.

Wetzel, D.T., Hauri, E.H., Saal, A.E., and Rutherford, M.J. (2015) Carbon content and degassing history of the lunar volcanic glasses. Nature Geoscience, 8, 755.

Figure Captions

Figure 1. A) and B) Backscatter electron and C) S-P-Na (R-G-B) maps that show the locations of analyses in thin section 12039,4 area 4. Black circles in panel A mark to the locations of cracks and pits that cross the analysis transect. Phases are labelled in panel B (Ap = apatite; S = sulfide; Fa = fayalite; Plag = plagioclase; Pyx = pyroxene; K,Ba-feld = K,Ba-feldspar; K-glass = K-rich mesostasis glass). In panel C, sulfide grains/blebs appear as red, apatite grains appear as green, and mesostasis glass appears as bright blue. The size of the beam is smaller than the symbol size. Hollow diamonds are saved stage motor positions that were not analyzed. Filled white, yellow, and red diamonds are analyzed positions. D) Calculated $S^{6+}/\Sigma S$ ratio from spectra at each analysis point from Fig. 1. Locations of cracks and pits near analysis points (see panel A) are marked by gray dashed lines. Dark gray field marks $S^{6+}/\Sigma S > 3\%$. Analytical uncertainties are smaller than symbol size.

Figure 2. A) Normalized S-XANES spectra for (top panel) gypsum (black curve), troilite (gray curve), and sulfide blebs in Apollo sample 12039,4 area 4 (red and yellow curves) and (bottom panel) epoxy in thin section 10044,33 (light green curve) and 12039,4 (dark green curve). B) S-XANES spectra for analysis points on apatite (q, n), mesostasis glass (i), and sulfide bleb (j). In panels A and B, the position of absorption peaks traditionally assigned to S^{2-} (2466, 2470, and 2478 eV) and S^{6+} (2482 eV) are marked in vertical black dashed lines. The black curves are data,

444 the green curves are synthetic spectra produced from linear combinations of spectra collected on
445 gypsum and troilite to provide a best fit to the data (see SI Appendix).
446
447 Figure 3. A) and B) Maps as in Fig 1 that shows the locations of analyses in thin section
448 10044,33. Colors in panel B are as in Fig 1. C) S-XANES spectra for analysis points on apatite.
449 The position of absorption peaks traditionally assigned to S^{2-} (2466, 2470, and 2478 eV) and S^{6+}
450 (2482 eV) are marked in vertical gray lines. All apatite measurements lack spectral evidence for
451 S^{6+} and thus have $S^{6+}/\Sigma S = 0$.
452
453 Figure 4. The relationship between $S^{6+}/\Sigma S$ ratios of igneous apatites and fO_2 at the time of apatite
454 crystallization from natural apatites (gray stars, this study) and experimentally grown apatites
455 (white stars, Konecke et al. 2017a). Error bars on gray stars represent the full range of $S^{6+}/\Sigma S$
456 ratios observed in measurements of lunar apatites and Durango apatite (i.e., lunar apatite
457 measurements yield $S^{6+}/\Sigma S$ ratios as high as 45%, but we hypothesize that the sulfate signal
458 originates from alteration or secondary mineralization after sample collection; Durango apatite
459 measurements show no spectral evidence of sulfide). Error bars on the experimentally grown
460 apatite data point reflect the full range of $S^{6+}/\Sigma S$ of apatite reported for that experiment
461 equilibrated at IW+3 (Konecke et al., 2017a). Also shown are the current accepted fO_2 ranges of
462 typical terrestrial and Martian magmas (black horizontal lines with arrows). Though in detail the
463 relationship between magmatic fO_2 and apatite $S^{6+}/\Sigma S$ ratios will likely have a dependence on
464 melt chemistry, the transition from sulfide-only to sulfate-only apatites appears to occur in a
465 narrow fO_2 range between ~IW+2 and ~IW+4, suggesting that a S-in-apatite oxybarometer could
466 be useful in constraining fO_2 in a variety of terrestrial and Martian igneous rocks.
467
468
469
471
472
473
474
475
476
477

This is a preprint, the final version is subject to change, of the American Mineralogist (MSA)
Cite as Authors (Year) Title. American Mineralogist, in press.
DOI: https://doi.org/10.2138/am-2019-6804

Figure 1

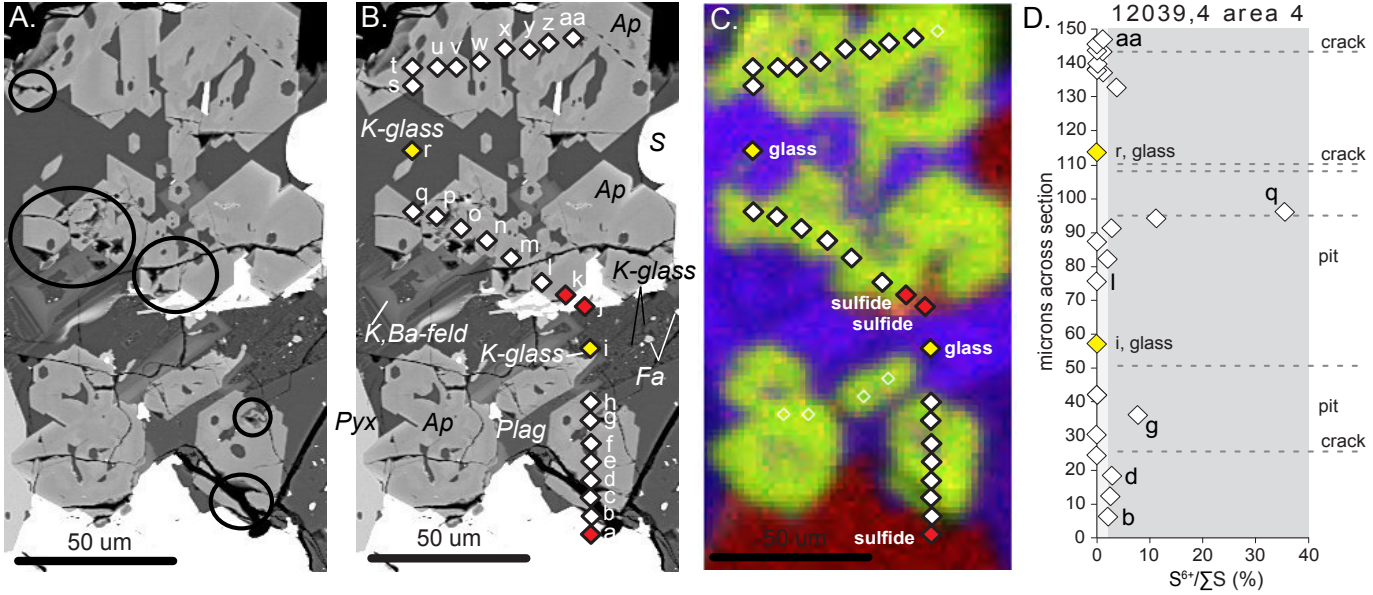

This is a preprint, the final version is subject to change, of the American Mineralogist (MSA)
Cite as Authors (Year) Title. American Mineralogist, in press.
DOI: https://doi.org/10.2138/am-2019-6804

Figure 2

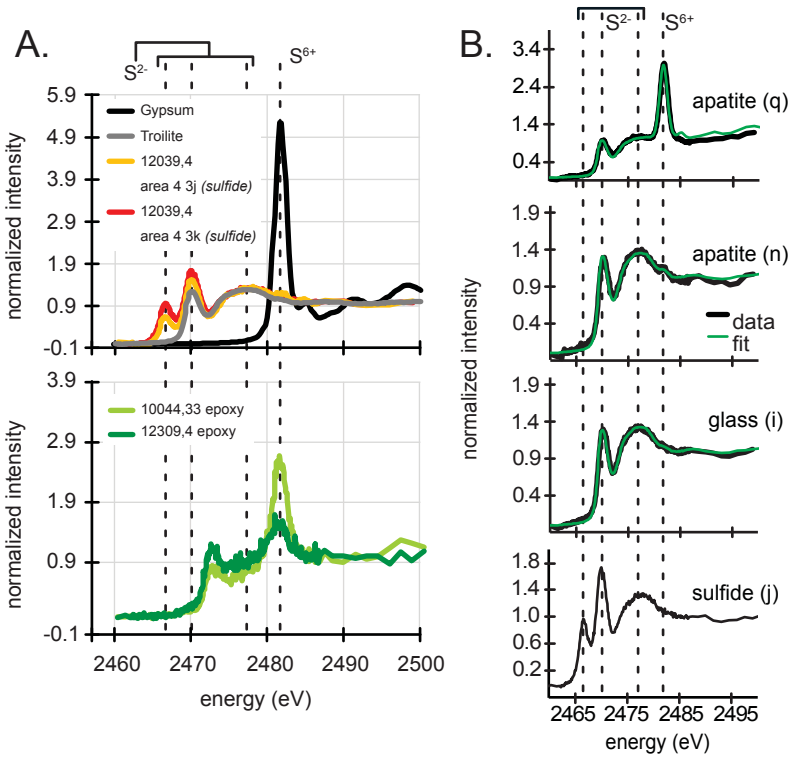

This is a preprint, the final version is subject to change, of the American Mineralogist (MSA)
Cite as Authors (Year) Title. American Mineralogist, in press.
DOI: https://doi.org/10.2138/am-2019-6804

Figure 3

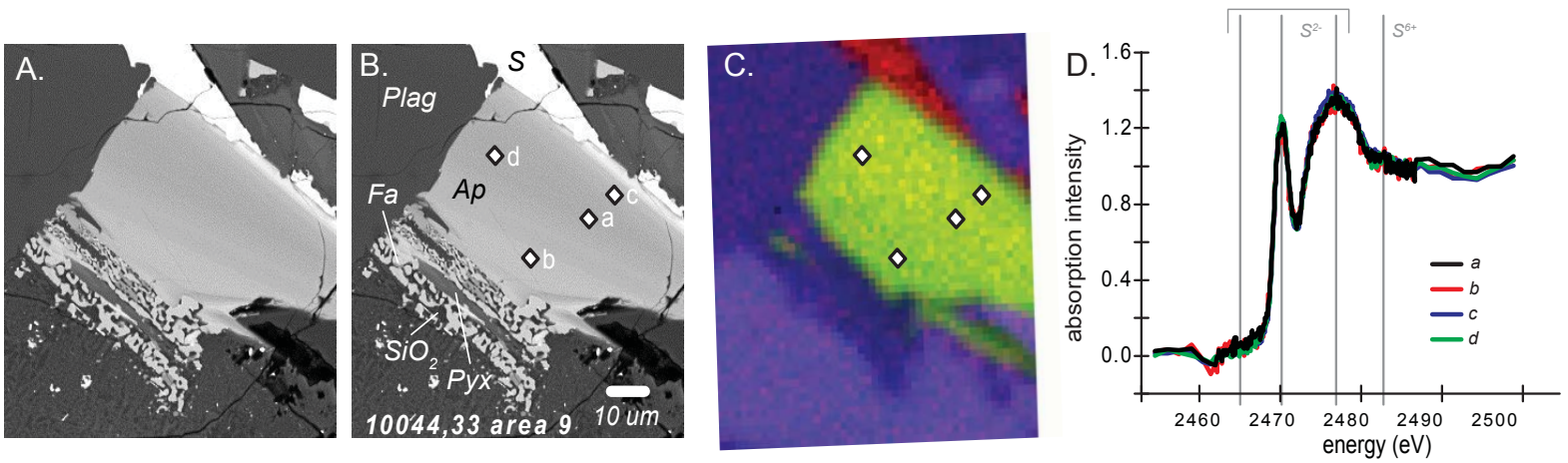

This is a preprint, the final version is subject to change, of the American Mineralogist (MSA)
Cite as Authors (Year) Title. American Mineralogist, in press.
DOI: https://doi.org/10.2138/am-2019-6804

Figure 4